Characteristics and Modeling of Harmonic Sources—Power Electronic Devices

Task Force on Harmonics Modeling and Simulation, IEEE PES Harmonic Working Group

***Abstract*—This paper presents a review of characteristics and modeling of major power electronic types of harmonic sources for the power system harmonic analysis. The power electronic switching types of harmonic sources to be reviewed include static power converters, static var compensators (SVCs), and cycloconverters. Discussions and comments for applications of these harmonic sources in harmonic modeling and simulation also will be described.**

***Index Terms*—Cycloconverter, harmonics, modeling, static converter, static var compensator, thyristor-controlled reactor.**

I. Introduction

THE PURPOSE of harmonic studies is to quantify the distortion in voltage and/or current waveforms at various locations in a power system. The need for a harmonic study may be indicated by excessive measured distortion in existing systems or by installation of harmonic producing equipment. One important step in harmonic studies is to characterize and to model harmonic-generating sources. Among the modern nonlinear loads, three-phase power electronic devices have a significant contribution in generating harmonics during their switching processes. Though the widely spread single-phase power electronic devices such as PCs, TVs, and battery chargers also generate currents rich in odd harmonics, the harmonic magnitudes are usually small and the phase angles are diversified. Harmonic modeling for their group effects generally requires statistical or probabilistic approaches. This topic will not be covered in the scope of the paper.

Many harmonic models have been proposed for representing three-phase power electronic devices [1]. The most common model is in the form of a harmonic current source, which is specified by its magnitude and phase spectrum. More detailed models become necessary if voltage distortion is significant or if voltages are unbalanced. Three basic approaches used to build detailed models include developing analytical formulae for the Fourier series as a function of terminal voltage and operating parameters for the harmonic source, developing analytical models for harmonic source operation and solving for its current waveform by a suitable iterative method, and solving for harmonic source steady-state current waveform with time-domain simulation.

Manuscript received May 22, 2000.

Task force members and contributors: R. Burch, G. Chang (editor, corresponding author), R. Dwyer, M. Grady, M. Halpin, C. Hatziadoniu, Y. Liu (editor), M. Marz, A. Medina, S. Middledanff, R. Natarajan, H. Nguyen, T. Ortmeyer, S. Ranade, P. Ribeiro (vice chair), D. Ruthman, T. Sims, N. Watson, J. Wikston, W. Xu (chair).

Publisher Item Identifier S 0885-8977(01)08509-0.

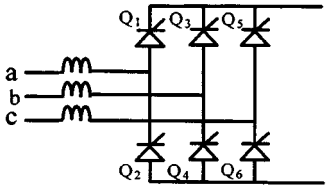

Fig. 1. The six-pulse line-commutated converter.

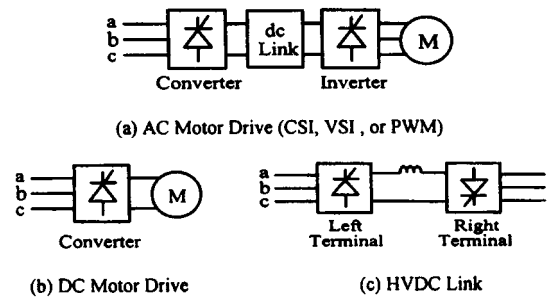

Fig. 2. Typical configurations of AC/DC motor drives and the HVDC link.

Commonly seen three-phase power electronic devices include static converters that are often used in HVDC links and motor drives, static var compensators, and cycloconverters. Harmonic current source models are frequently used to represent these devices. These devices are sensitive to supply voltage distortion and unbalance. For large power electronic devices such as HVDC terminals and transmission level SVCs, detailed three-phase models may be needed. Factors such as firing-angle dependent harmonic generation, supply voltage unbalance and distortion are required to take into account in the model. These studies normally scan through various possible operating conditions of the device and filter performance.

II. Three-Phase Line-Commutated Converters

The introduction of line-commutated converters has caused a significant increase in harmonic-generating loads. The device is most usual operated as a six-pulse converter, as shown in Fig. 1, or configured in parallel arrangements for high-pulse operations. Major applications of these converters are to be used as a front-end in ac/dc adjustable speed drives (ASDs) and HVDC links. Typical circuit configurations for these devices are shown in Fig. 2. The two types of commonly used converter circuits are the thyristor and the rectifier bridges. The former is usually used in HVDC links, current-source ac drives, and dc drives, while the later is normally seen in voltage-source and PWM ac drives.

The three key components in the most popular types of ac motor drives are the converter section (front-end), the inverter

section, and the dc circuit that connects the two sections [2]. The converter section changes the ac 60 Hz line voltage into dc voltage. Through the switching process, it will inject harmonic currents into the power system. The dc circuit is called the dc link. The dc link current also contains harmonic ripples because of the conversion process. The ripples then can penetrate into the power system. The inverter section is used to change the dc voltage into adjustable frequency of voltage to the ac motor. The inverter can introduce additional ripples into the dc link current, which in turn injects into the supply system side. In general, the extent and the frequency of inverter-produced ripples are largely a function of inverter design and motor parameters.

A. Characteristics of Harmonics Generated by the Three-Phase Line-Commutated Converter

In Fig. 1, for the ideal three-phase operation with a constant output current (I_d) and assuming zero firing angle ($\alpha = 0$) and no commutation overlap ($\mu = 0$), the converter load draws currents from the source that consists of equally separated positive and negative rectangular-shape currents. It can be shown that the phase-a input current is as given in (1).

$$i_a(t) = \sum_h \left(\sqrt{2}I_1/h\right) \sin\left(h\omega_1 t + \delta_h\right), \qquad (1)$$

where $h = 1, 5, 7, 11, 13, \ldots$ [3]. Thus, the ac harmonic currents generated by a six-pulse converter include all odd harmonics except triplens. Characteristic harmonics generated by converters of any pulse number are in the order of $h = pn \pm 1$, where $n = 1, 2, \ldots$ and p is the pulse number of the converter. In the case of nonzero firing angle and nonzero commutation overlap ($\mu \leq 60°$), [4] shows that the rms value of each characteristic harmonic current can be determined by

$$I_h = \sqrt{6}I_d F(\mu, \alpha)/\{\pi h[\cos\alpha - \cos(\alpha + \mu)]\}, \qquad (2)$$

where $F(\mu, \alpha)$ is an overlap function. According to (1) and (2), the converter harmonic current magnitudes decrease according to $1/h$ rule under the ideal operation. However, if 1) the converter input voltages are unbalanced or 2) unequal commutating reactances exist between phases or 3) unequally spaced firing pulses are present in the converter bridge, the converter will produce noncharacteristic harmonics in addition to the characteristic ones.

In practice, for the power electronic equipment in Fig. 2 that employ the line-commutated converters as front ends, the characteristics of generated harmonic currents are not the same. This is due to the fact that the components connected to the converter output stage are different. For instance, a HVDC link typically has a smoothing reactor connected to the converter output, which provides low ripple in the dc current. A dc motor drive depends on armature inductance to smooth the current, and will have higher ripple levels. AC drives which omit any dc link reactors can have still higher levels of ripple. The dc ripples could cause the converter ac input current significantly to deviate from the ideal. Fig. 3 shows typical converter input current waveforms of ac/dc motor drives and the HVDC link.

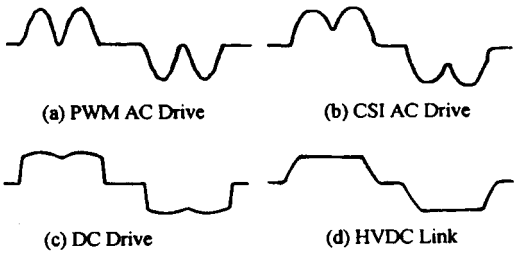

Fig. 3. Typical converter input current waveforms of AC/DC motor drives and the HVDC link.

B. Harmonic Models of the Three-Phase Line-Commutated Converter

In general, a three-phase line-commutated converter can be simply represented by a harmonic current source or a model that takes into account the interaction between the ac source network and the converter dc system. When the latter situation is considered, a more sophisticated converter analysis for the resulting harmonic currents as a function of system reactance, firing angle, and commutation angle is required. The accuracy of converter model needs also to be considered to guarantee the convergence of the simulation. At present, there are several techniques that have been developed for modeling of the converter in harmonic simulation. These models can be categorized as frequency-domain and time-domain based models. The frequency-domain models are further divided into current source model, transfer function model, Norton-equivalent circuit model, harmonic-domain model, and three-pulse model. Time-domain models include representing the converter by a set of differential equations and the state-space model. Some of these models can be integrated in harmonic power flow analysis while the others are not. The following sections give an overview on these converter models.

1) Current Source Model: The most common technique for harmonic simulation is to treat the converter as known sources of harmonic currents with or without including phase angle information. This is due to the fact that the converter acts as an injection current source to the system in many operational conditions. Generally, the steady-state condition is assumed. As given in (3), the current harmonics injected into a bus have a magnitude determined from the typical measured spectrum and rated load current for the harmonic source, where the subscript "*sp*" indicates the typical harmonic current spectrum of the source [1]. The frequency-domain nodal equations for each harmonic are used to compute the network harmonic voltages via the system harmonic admittance or impedance matrix. The superposition is then applied to convert the solved values of all harmonic voltages into the time domain at each network bus. This model applies to both balanced and unbalanced converter systems [5]–[8]. For harmonic studies involving one converter, the phase angles are ignored and only the magnitudes are used in the harmonic simulation. However, harmonic phase angles need to be included when multiple sources are considered simultaneously for taking the harmonic cancellation effect into account.

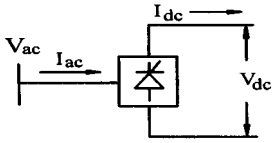

Fig. 4. A simplified schematic converter model.

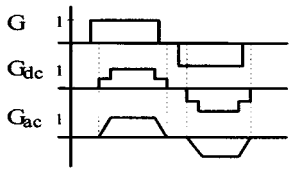

Fig. 5. Voltage and current transfer functions with firing angle variation and commutation overlap.

In such case, (4) can be used to determine the harmonic phase angle, θ_h, and a conventional load flow solution is needed for providing the fundamental frequency phase angle, θ_1 [1].

$$I_h = I_{rated} \cdot I_{h-sp}/I_{1-sp} \tag{3}$$

$$\theta_h = \theta_{h-sp} + h(\theta_1 - \theta_{1-sp}). \tag{4}$$

The advantages of the current source method are that the solution can always be obtained directly (noniterative) and it is computationally efficient. Ideally, this method is able to handle several harmonic sources simultaneously. The drawback of this method is that typical harmonic spectra are often used to represent the harmonic currents generated by the converter that ignores the interaction between the network and the converter. This prevents an adequate assessment of cases involving nontypical operating modes, such as partial loading, excessive harmonic voltage distortions and unbalanced network conditions. Reference [5] suggests that the current injection model should be used carefully (if at all) when the converter source voltage THD is on the order of 10% or more.

Many other models, both in the time domain and in the frequency domain, have been proposed to overcome the aforementioned drawbacks. In each of these models, it couples the converter with the system admittance matrix, or some other more complicated expressions of the power system. Iterative algorithms, either sequentially or simultaneously, are generally required to obtain the final solution. In the commonly used iterative harmonic analysis (IHA), the initial estimate of harmonic current injections at the converter is determined first and the network bus harmonic voltages are computed. A new estimate of the harmonic injection currents is then obtained from the computed harmonic voltages. This process is sequentially repeated until convergence in the magnitude of the harmonic voltages on each network bus is reached. In the power flow type of harmonic analysis, the active power and reactive power of the converter are specified in advanced as an operating point, the Newton–Raphson algorithm is then applied to simultaneously updating the harmonic voltages and control variables via the linearization around the specified converter operating point. These more complex converter models are reviewed below.

2) Transfer Function Model: The simplified schematic circuit, as shown in Fig. 4, can be used to describe the transfer function model of a converter. [9]–[13] present similar concepts based on the modulation theory that uses two transfer functions, $G_{\varphi,\,\mathrm{dc}}$ and $G_{\varphi,\,\mathrm{ac}}$, to relate the dc and ac sides of the converter. Fig. 5 shows the two transfer (switching) functions, $G_{\varphi,\,\mathrm{dc}}$ and $G_{\varphi,\,\mathrm{ac}}$, where G is the ideal transfer function without considering firing angle variation and commutation overlap. As shown in (5), the dc voltage is directly computed by summing each input phase voltage, V_φ, multiplied by its corresponding transfer function.

$$V_{\mathrm{dc}} = \sum_{\varphi} G_{\varphi,\,\mathrm{dc}} V_\varphi, \qquad \varphi = a,\, b,\, c. \tag{5}$$

Each input phase current of the converter can be expressed as

$$i_\varphi = G_{\varphi,\,\mathrm{ac}} i_{\mathrm{dc}}, \qquad \varphi = a,\, b,\, c. \tag{6}$$

In (5) and (6), the two transfer functions can include the deviation terms of the firing angle and commutation overlap, where the current transfer function is approximated by linear ramp during commutation. In addition, the effects of converter input voltage distortion or unbalance and harmonic contents in the output dc current can be modeled as well. This allows the prediction of voltage distortion on the dc side and current distortion on the ac side of the converter simultaneously.

In [14], the authors propose efficient techniques by linearizing the interaction between the converter dc system and the ac network at different converter operating points of interests. The entire system is then solved via the harmonic coupling matrix equation to account for the interaction, where the harmonic coupling matrix equation is expressed as

$$\begin{bmatrix} \mathbf{I_{ac}} \\ \mathbf{V_{dc}} \end{bmatrix} = \begin{bmatrix} \mathbf{A} & \mathbf{B} & \mathbf{E} \\ \mathbf{C} & \mathbf{D} & \mathbf{F} \end{bmatrix} \begin{bmatrix} \mathbf{V_{ac}} \\ \mathbf{I_{dc}} \\ \boldsymbol{\alpha} \end{bmatrix}. \tag{7}$$

$\mathbf{I_{ac}}$ and $\mathbf{V_{ac}}$ in (7) are vectors of ac side sequence harmonic currents and voltages. $\mathbf{I_{dc}}$ is the vector of dc side harmonic currents, and $\boldsymbol{\alpha}$ is the firing angle harmonics. $\mathbf{A}$, $\mathbf{B}$, $\mathbf{C}$, $\mathbf{D}$, $\mathbf{E}$, and $\mathbf{F}$ can be regarded as sub-matrices of the converter transfer functions between associated input and output variables and are obtained by the time-domain simulation with harmonic perturbations. These matrices are built for each operating point under consideration and are then combined with the ac and dc system impedance as well as control characteristics at harmonic frequencies.

Without considering firing angle harmonics, [9] and [15] also develop a similar model of (7) with only sub-matrices $\mathbf{A}$, $\mathbf{B}$, $\mathbf{C}$, $\mathbf{D}$ are used to relate voltages and currents in converter ac and dc sides. The model is used to determine the frequency-dependent impedance for a converter. As given in (8) and (9), the ac and dc sides of the converter are modeled by a frequency-dependent Thévenin source and by a frequency-dependent Norton source, respectively. $\mathbf{V_{ach}}$ and $\mathbf{I_{dch}}$ are vectors of the ac-side harmonic voltage source and the dc-side harmonic current source. $\mathbf{Z_{ac}}$ and $\mathbf{Z_{dc}}$ are diagonal matrices of ac and dc side harmonic

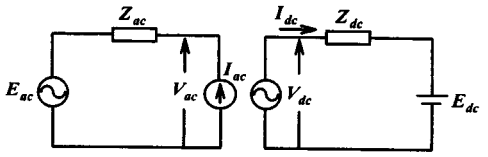

Fig. 6. Converter AC- and DC-side harmonic Thévenin equivalent circuits.

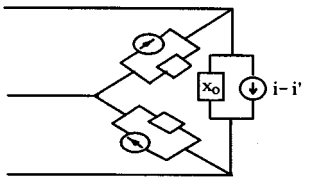

Fig. 7. The converter Norton-equivalent circuit.

impedance. This model includes the effects of variations in firing angles and in commutation times.

$$\mathbf{V_{ac}} = \mathbf{Z_{ac}}\mathbf{I_{ac}} + \mathbf{V_{ach}} \tag{8}$$

$$\mathbf{I_{dc}} = \mathbf{V_{dc}}/\mathbf{Z_{dc}} + \mathbf{I_{dch}}. \tag{9}$$

By combining the above two matrix equations with $\mathbf{A}$, $\mathbf{B}$, $\mathbf{C}$, $\mathbf{D}$ relations, the ac and dc side frequency-dependent impedance, $\mathbf{V_{ac}}/\mathbf{I_{ac}}$ and $\mathbf{V_{dc}}/\mathbf{I_{dc}}$, of the converter are obtained. This model is suitable for harmonic filter design where the harmonic analysis can be substantially simplified.

Under the assumptions of continuous dc current and equidistant firing scheme, [16] and [17] also present harmonic coupling matrix techniques for line commutated converters. Therefore, the matrix of (7) only shows the coupling between the converter voltage and current harmonics, where sub-matrices $\mathbf{A}$, $\mathbf{B}$, $\mathbf{C}$, and $\mathbf{D}$ are functions of converter firing angles, commutation inductance, and commutation angles. The commutation times are determined by the boundary conditions describing the currents through each thyristor pair ceased to zero. Since converter voltages, currents, and switching functions are represented by the complex Fourier series, each sub-matrix is infinite dimensional. In practice, when considering the interaction between the converter and the power system, both of the converter and the power system can be represented by their harmonic Th,venin equivalent circuits, as shown in Fig. 6. Then, the relation of (10) holds.

$$\begin{bmatrix} \mathbf{E_{ac}} \\ \mathbf{E_{dc}} \end{bmatrix} = \begin{bmatrix} \mathbf{I} - \mathbf{Z_{ac}}\mathbf{A} & -\mathbf{Z_{ac}}\mathbf{B} \\ \mathbf{C} & \mathbf{D} + \mathbf{Z_{dc}} \end{bmatrix} \begin{bmatrix} \mathbf{V_{ac}} \\ \mathbf{I_{dc}} \end{bmatrix}, \tag{10}$$

where

- $\mathbf{Z_{ac}}$ and $\mathbf{Z_{dc}}$ diagonal and of infinite dimensions denoting the Thévenin ac and dc impedance;
- $\mathbf{I}$ identity matrix;
- $\mathbf{E_{ac}}$ and $\mathbf{E_{dc}}$ known vectors of infinite dimension representing the Thévenin ac and dc voltage sources.

The ac current and dc voltage harmonics are solved with the incorporation of an iterative approach. The proposed model is developed for both balanced single-phase and three-phase converters while ignoring the effects of commutation and firing angle variations.

Assuming the commutation angle is known and the system is balanced, [18] also develops an ac side equivalent circuit-based method by the use of transfer function approach for the six-pulse converter. Since the dc side parameters and the control of the converter can be integrated in the ac side equivalent circuits, it is shown that the proposed approach is particularly useful when the dc side information of the converter is not required. The approach is computationally efficient and is more suitable for harmonic studies when the power system contains multiple converters.

3) Norton-Equivalent Circuit Model: In the iterative harmonic analysis, the converter is usually represented by a fixed harmonic current source at each iteration. For better convergence, the Norton equivalent can be used for the converter. The nonlinear relationship between converter input currents and its terminal voltages are expressed by

$$\mathbf{I} = f(\mathbf{V}), \tag{11}$$

where $\mathbf{I}$ and $\mathbf{V}$ are harmonic vectors. When considering a relatively small content of harmonics in the converter terminal voltages, it is possible to linearize the behavior in the vicinity of the converter base operating point, ($\mathbf{V_b}$, $\mathbf{I_b}$). The $\mathbf{I}$–$\mathbf{V}$ dependency of the converter then can be expressed as

$$\mathbf{I} = \mathbf{Y_J}\mathbf{V} + \mathbf{I_N}, \tag{12}$$

where $\mathbf{I_N} = \mathbf{I_b} - \mathbf{Y_J}\mathbf{V_b}$ is called the Norton equivalent and where $\mathbf{Y_J}$ is the Norton admittance matrix representing the linearization [19].

References [20]–[22] propose a three-phase harmonic Norton-equivalent circuit model which is developed to represent the converters of HVDC links and ac/dc motor drives under both unbalanced and distorted input conditions. This model is also suitable for various drive operating conditions. It assumes that no coupling between equivalent circuits at different harmonic frequencies. A common approach for this model is to have the converter switching process represented by a switching function whose frequency-domain expression is obtained by the use of discrete Fourier transform. The ac side harmonic phasors are then obtained via the convolution of the switching function and the dc side harmonic phasors. This model is then iteratively improved in a frequency-domain network solution process via solving the network nodal equations for each harmonic of interests. Once the nodal voltages are obtained, improved values for the equivalent harmonic current sources can be calculated which in turn used to compute improved voltages. The solution process stops when the changes in the Norton-equivalent current sources are sufficiently small.

Fig. 7 shows the proposed three-phase equivalent delta-connected converter Norton-equivalent circuit model, where the Norton admittance represents an approximation of the converter response to variations in its terminal voltage harmonics or unbalance. As shown in Fig. 7, if the circuit is used to represent HVDC converter, i, i', and x_o represent the switching current without commutation overlap, the commutation overlap current, and the commutation overlap reactance for a branch, respectively [20]. The impedance x_o is served as a return path

for mismatching currents and prevents singularity of system admittance matrix during the iterative solution process. For ac/dc drive converter model, $i - i'$ is the supply-voltage-dependent harmonic current source and x_o is the equivalent harmonic impedance [21], [22]. The converter dc current is determined with a given dc link voltage. This voltage may change if newly calculated dc link current is used to compute the voltage. A sub-iteration is needed to obtain accurate dc link voltage and current. Provided with dc link data, this model is also suitable for the three types of ASDs.

4) Harmonic-Domain Model: A harmonic-domain model that formulates a general set of nonlinear equations describing the converter in steady state is developed in [23]–[25]. In the proposed method, it analyzes the converter by observing the converter passing through a sequence of twelve states describing its conduction pattern. Assuming the converter is lossless, the converter in each state can be represented by a passive linear circuit and can be analyzed by means of complex harmonic phasors. Under normal operation, the overall state of the converter is specified by the angles of the state transition. These angles are the switching instants corresponding to the six firing angles and the six ends of commutation angles, where these angles are determined by their corresponding nonlinear mismatch equations solved by Newton method. The converter response to an applied terminal voltage is characterized via convolutions in the harmonic domain. The dc voltage is obtained by solving each of the twelve linear circuits for dc voltage samples. The overall dc voltage, as given in (13), is obtained by convolving the twelve voltage samples, $V_{k,p}$, with their corresponding square pulse sampling functions, ϕ_p, which have a value of one during the appropriate state, and a value of zero during all other states. The period of the sampling function is the same as that of the fundamental.

$$V_d = \sum_{p=1}^{12} V_{k,p} \otimes \Phi_p = \sum_{h=1}^{H} \sum_{n=1}^{2H} V_{k,p}^{h} \Phi_p^{n}, \qquad (13)$$

where H is the highest harmonic order under consideration. The converter input currents are obtained in the same manner using the same sampling functions. In the proposed model, because no Fourier transform is required, the convolution process is computationally efficient. The use of sampling functions is similar to other work using the switching function. Because this model takes only one cycle of ac input voltage as the fundamental, and so only harmonics are analyzed. If necessary, this model can be extended to the steady state over several cycles that allow inter-harmonics to be solved.

5) Three-Pulse Model: In the HVDC harmonic analysis, conventional converter models usually assume no current path between the ground, the pole, and converter neutral terminals [4]. Under such assumptions, the dc side voltage harmonics are of the order of $6n$ or $12n$ times the fundamental frequency, where n is an integer. However, due to the existence of stray capacitance inherent in the converter transformer, smooth reactors, bushes, and buswork, [26] and [27] report that significant amount of odd-triplen harmonic currents are monitored in the

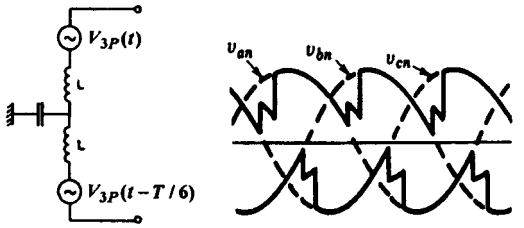

(a) 3-Pulse Model (b) Upper and Lower 3-Pulse Voltage Sources

Fig. 8. The six-pulse converter modeled with two 3-pulse voltage sources.

electrode lines and the pole of the HVDC system that can not be analyzed by the conventional model.

Reference [28] proposes a 3-pulse model which includes the current path provided by the stray capacitance of the HVDC converter. Assuming ideal input voltages, the dc side voltage of the six-pulse converter is decomposed into two 3-pulse voltage sources (upper and lower) explaining the generation of all odd harmonics plus those multiples of six. Fig. 8 shows the six-pulse converter modeled with two 3-pulse voltage sources on its dc side and the corresponding waveforms. For the twelve-pulse converter, it can be modeled with four 3-pulse voltage sources. Based on the 3-pulse model, an analytic solution for describing the harmonic transfer in a HVDC converter with taking into account the effects of unbalanced and distorted input voltages is also shown in [29].

6) Time-Domain Model: In the time domain, a converter can be expressed as a set of differential equations or state equations that govern its performance. After solving these equations, the harmonic spectra of converter input currents are generally found by the use of Fourier method such as fast Fourier transform [30]–[33]. This device model usually can be integrated with frequency-domain network model for harmonic power flow analysis or used in a time-domain simulation including the power system.

Assuming the system is balanced, similar models are proposed in [34] and [35] that analytically derive and solve a set of differential equations associated with the converter input currents over six conduction and commutation intervals in a half cycle of the fundamental frequency. The input currents are then converted into frequency domain by the use of Fourier series. For considering the interaction between the converter and the power system, the harmonic currents are injected into the power network with the incorporation of conventional Newton–Raphson type of power flow algorithm including the converter load. The harmonic voltages at each network bus are then simultaneously solved.

Reference [36] presents a state-space model that includes the system frequency-dependent impedance with the converter which can be used in iterative harmonic analysis to improve convergence. Non-ideal conditions such as input source unbalance, distortion, and uneven firing angles can be taken into account in the model. It assumes that the time evolution of the converter input current can be obtained by considering the full conduction and commutation intervals for normal operation. As shown in Fig. 9, with introducing a pseudo parameter, w,

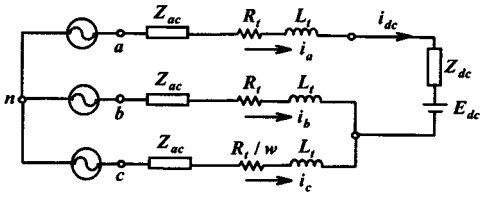

Fig. 9. The simplified converter circuit.

in the simplified circuit (w is one for commutation state and is zero for full conduction state), the state equations describing the circuit is derived as (14).

$$\mathbf{D}(p)\mathbf{i} = \mathbf{B}(w)\mathbf{v} - \mathbf{b}E_{\rm dc}, \tag{14}$$

where

- p differential operator;
- $\mathbf{i}$ vector representing the conduction and commutation currents to be determined;
- $\mathbf{v}$ vector representing input phase voltages;
- $\mathbf{B}(w)$ constant matrix;
- $\mathbf{D}(p)$ matrix where its elements are functions of ac and dc source frequency-dependent impedance and of the converter transformer impedance.

Once the conduction and commutation currents in (14) are found, the converter input currents are then directly derived. The dc voltage can be found in the same manner. The same authors further extend their proposed model to deal with multiple-converter cases in [37].

A state-space model for the converter which is modeled as an equivalent nonlinear current source is also proposed in [38]. It allows computing the overall harmonic current generated in a multiple-converter system through an iterative process, where nonlinear current sources corresponding to all converters are determined by calculating the input current to each converter with only one converter supplied by the source system one at a time. The process stops once the relative current tolerance for each converter is reached. In this model the source system is expressed as its Thévenin equivalent.

III. Static Var Compensator

The static var compensator (SVC) is used as a voltage controller that dynamically controls network voltages by adjusting the amount of reactive power supplied to or absorbed from the power system. As shown in Fig. 10(a), the configuration of a single-phase SVC consists of shunt capacitors with a thyristor-controlled reactor (TCR). The TCR is a reactor in series with a pair of anti-parallel thyristors, where each thyristor conducts alternatively in half cycle of the supply frequency. The duration of conduction depends on the thyristor firing angle, α, and thus adjusts the reactive power supply or absorption. Referred to the fundamental voltage positive-going zero-crossing point, the interval of conduction is defined as $\sigma = 2(\pi - \alpha)$ and ranges from full conduction at $\alpha = \pi/2$ to zero conduction at $\alpha = \pi$. Harmonic currents are generated for any conduction intervals within the two firing angles. Fig. 10(b) shows a typical current waveform generated by a TCR branch, where the dash line represents the supply voltage. It is noted that the conduction intervals of the two thyristors can be different. The harmonic characteristics and models of the TCR are further described as follows.

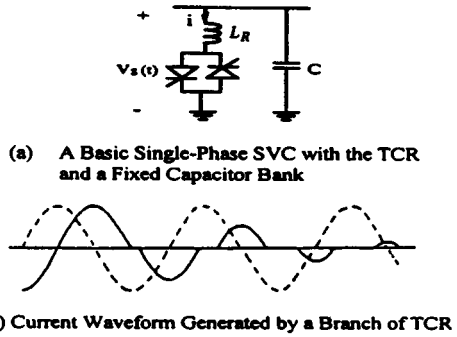

(a) A Basic Single-Phase SVC with the TCR and a Fixed Capacitor Bank

(b) Current Waveform Generated by a Branch of TCR

Fig. 10. The SVC configuration and typical TCR current waveform.

A. Characteristics of Harmonics Generated by the TCR

With the ideal supply voltage, the generated rms harmonic currents in the TCR of Fig. 10(a) are functions of the thyristor firing angle, α, and are given by (15).

$$I_h(\alpha) = \frac{4V_1}{\pi\omega L_R}\left[\frac{\cos\alpha\sin(h\alpha) - h\cos(h\alpha)\sin\alpha}{h(h^2-1)}\right], \tag{15}$$

where $h = 3, 5, 7, \ldots, \sigma$ is the conduction angle, and L_R is the inductance of the reactor [39], [40]. From Fig. 10(a) and (15), we see that all odd harmonics are present in the input current for the TCR. In the balanced three-phase application, three single-phase TCRs are usually in delta connection. Therefore, the triplen currents circulate within the delta circuit and do not enter the power system that supplies the TCRs.

When the single-phase TCR is supplied by a nonsinusoidal input voltage, $v_s(t) = \sum_h V_h \sin(h\omega t + \phi_h)$, the current through the compensator can be obtained by solving $v_s(t) = L_R di/dt$ and is proved to be the discontinuous current in (16).

$$i(t) = \begin{cases} \displaystyle\sum_h \frac{V_1}{h\omega L}\left[\cos(h\alpha + \phi_h) - \cos(h\omega t + \phi_h)\right], \\ \qquad\qquad \dfrac{\alpha}{\omega} \le t \le \dfrac{\alpha+\sigma}{\omega} \\ 0, \\ \qquad\qquad 0 < t < \dfrac{\alpha}{\omega} \text{ and } \dfrac{\alpha+\sigma}{\omega} < t < \dfrac{\alpha+\pi}{\omega} \end{cases} \tag{16}$$

B. Harmonic Models of the TCR

Harmonic models of a TCR can be categorized in frequency and time domains. The frequency-domain models include current source model, Norton-equivalent model, and transfer function model. The time-domain models include state-space model and those conventional time-domain models that represent the TCRs as a set of differential equations.

1) Current Source Model: The harmonic contents of (16) can be obtained with the use of discrete Fourier analysis for the given supply voltage, which produces the harmonic currents expressed by $i_h(t) = \sum_h I_h \sin(h\omega t + \theta_h)$, and they can be used as a current source model for the TCR [41]. Reference [42] also

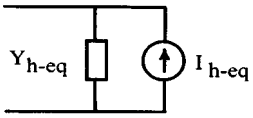

Fig. 11. Norton-equivalent circuit of a branch of the TCR.

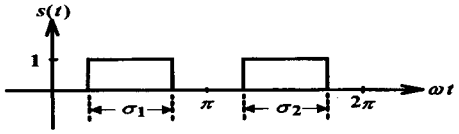

Fig. 12. The TCR thyristor switching function.

proposes a similar model based on Fourier transform which corresponds to the real and imaginary parts of the harmonic current at each order.

2) Norton-Equivalent Models: Reference [43] presents a Norton-equivalent model for the delta-connected TCRs when the input voltage is unbalanced and is used in a harmonic power flow analysis. It is assumed that no coupling between the Norton-equivalent circuits at different harmonics and the conduction angle of the TCR is known. Fig. 11 shows the Norton-equivalent circuit of the TCR given in Fig. 9 for the hth harmonic, where $\mathbf{Y}_{h-eq} = (jh\omega L_{eq})^{-1}$ and $\mathbf{I}_{h-eq} = \mathbf{V}_h/(jh\omega L_{eq}) - \mathbf{I}_h$, and where $\mathbf{V}_h = V_h\angle\phi_h$, $\mathbf{I}_h = I_h\angle\theta_h$, and $L_{eq} = \pi L_R/(\sigma - \sin\sigma)$ is the equivalent inductance of the TCR branch. The harmonic current phasors, $\mathbf{I_h}$, can be obtained via Fourier analysis of (16) for a given TCR input voltage, and then are used to compute the equivalent harmonic current phasors, $\mathbf{I_{h-eq}}$, and network harmonic voltages through harmonic admittance matrix. An iterative process is continued until the convergence criteria are met.

A similar approach is shown in [44] and [45] which linearizes the nonlinear inductor of the three-phase delta-connected TCR as a harmonic-domain voltage-dependent Norton-equivalent circuit, where the asymmetrically gated control action is included. Initially, the TCR current of Fig. 10 is modeled with the time-domain dynamic equations, as given in (17), where $s(t)$ is the thyristor switching function with values of one and zero which represent conduction states and is shown in Fig. 12. The Fourier transform is then applied to (17) by taking the integration and discrete convolution to obtained the frequency-domain TCR current. Next, the Norton-equivalent harmonic model of the single-phase TCR is developed and the three-phase Norton-equivalent is determined by the power invariant transformations. In the proposed model, the harmonic coupling between different Norton-equivalent circuits is taken into account through the computed harmonic admittance matrix and then the TCR harmonic currents are solved. This model is suitable for directly incorporation into frequency-domain Newton–Raphson type harmonic power flow analysis.

$$\frac{di}{dt} = s(t)v_s(t)/L_R \tag{17}$$

For improving computational efficiency, [46] presents a Norton-equivalent model of the three-phase TCR in Hartley's domain, where unbalances in input voltages, firing angles and inductances are taken into account. It is showed that harmonic solutions obtained using Hartley's frame-of-reference can be two to four times faster that of using Fourier's frame-of-reference.

3) Transfer Function Model: In [47] an approach used to compute the harmonics generated by a naturally commutated single-phase TCR in the complex conjugate phasor space is proposed, where the coupling of harmonics in TCR switching circuit through the system impedance is taken into account. In the model the TCR supply voltage, the thyristor switching function in Fig. 12, reactor admittance, and system impedance are represented by their corresponding complex Fourier series, $\mathbf{V_S}, \mathbf{S}, \mathbf{Y_R}$, and $\mathbf{Z_S}$, respectively. Observing Fig. 10, the voltage across the reactor and the TCR current can be expressed as

$$\mathbf{V_R} = \mathbf{S}\mathbf{V_S} \tag{18}$$

and

$$\mathbf{I_R} = \mathbf{Y_R}\mathbf{V_R} = \mathbf{Y_{TCR}}\mathbf{V_S} \tag{19}$$

where $\mathbf{Y_{TCR}} = \mathbf{Y_R}\mathbf{S}$ can be thought of TCR harmonic admittance matrix or transfer function. Incorporating the supply system with (18), (19), and commutation boundary conditions, the TCR current that includes the interaction with the supply system can be obtained. In this model the power system is assumed balanced and is represented by a harmonic Th,venin equivalent. An iterative procedure is used to compute the harmonic voltages and currents of the TCR.

Reference [48] also presents a transfer function model that uses Walsh transformation for computing the three-phase TCR input current harmonics. In the model the TCR transfer function is the developed harmonic admittance matrix consisted of Walsh Norton-equivalent admittance and TCR admittance matrix without including the supply system Thévenin equivalent. Not like the complex algebra is used in Fourier series and Hartley series, only the real algebra is used in Walsh domain. Hence, a more efficient solution is expected. In [49] the authors develop a three-phase TCR transfer function model to compute the TCR current harmonics in the frequency domain, where the transfer function is the switching function that relates the supply line voltage and the reactor voltage as given in (18). In the model the spectra of the transfer functions associated with supply voltage distortions and firing angle deviations are determined by performing a pulse duration modulation [9]. The TCR current harmonics are then computed by integrating (17) in the frequency domain. The linearized frequency-domain TCR model is suitable for both integer and noninteger harmonics.

4) Time-Domain Model: Reference [47] also introduces a state-space model for a single-phase SVC that includes a fixed capacitor in parallel with the TCR, as shown in Fig. 13, where the power system is represented by its Thévenin equivalent. The matrix form of the state equations can be expressed as (20),

$$\begin{bmatrix} \dfrac{dv_c}{dt} \\ \dfrac{di_c}{dt} \end{bmatrix} = \begin{bmatrix} 0 & 1 \\ -\left(\dfrac{1}{L_S} + \dfrac{s}{L_R}\right) & 0 \end{bmatrix} \begin{bmatrix} v_c \\ i_c \end{bmatrix} + \begin{bmatrix} 0 \\ \dfrac{1}{L_S} \end{bmatrix} V_s, \tag{20}$$

where s is the switching function given in (17). Using the linear system theory, the above periodic time-varying system can be

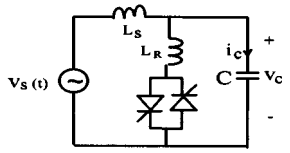

Fig. 13. The simplified single-phase SVC circuit.

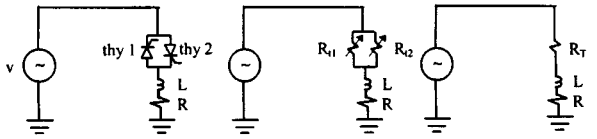

Fig. 14. The equivalent circuit for the TCR.

solved and the resonant condition of the circuit is also identified. The TCR harmonic currents are computed accordingly. This model can be easily extended to the three-phase TCR case.

As shown in Fig. 14, [50] proposes a time-domain TCR model that the two anti-parallel thyristors are replaced by two time-varying resistors, R_{t1} and R_{t2}. An equivalent resistance, R_T, is then used to represent these resistors. R_T becomes zero when any of the thyristors is conducted. Therefore, the TCR state equation is expressed by

$$\frac{di}{dt} = \frac{v}{L} - \frac{R + R_T}{L} i \tag{21}$$

and is efficiently solved by the use of a novel Newton method for speeding the convergence of the TCR current. In addition, two general time-domain SVC models based on the nodal analysis that integrated in EMTP to predict possible harmonic interactions between the SVC and its supply system are also proposed in [51] and [52]. In both models efficient initialization methods are used to improve the solutions.

IV. Cycloconverter

Cycloconverters are usually used in low-speed and high-power applications for controlling the speed of ac motors. A cycloconverter is a frequency changer that directly converts ac power at one input frequency to output power at a different frequency without the requirement of a dc link, where the output frequency is usually limited to one-third of the input frequency for reducing the output harmonics. Two major modes of cycloconverter operations are noncirculating current mode and circulating current mode. The former usually generates significant harmonic currents into the connected power system. In Fig. 15, it shows a commonly seen 6-pulse, 3-phase to 3-phase cycloconverter connected to the stator of an ac motor. As shown in Fig. 15(a), each phase contains two anti-parallel six-pulse converters. One converter supplies current $i+$ for the positive half-wave of the stator current and the other $i-$ for the negative half-wave. Fig. 15(b) shows the input current of one phase.

A. Characteristics of Harmonics Generated by Cycloconverters

A cycloconverter generates very complex frequency spectrum that includes sidebands of the characteristic harmonics.

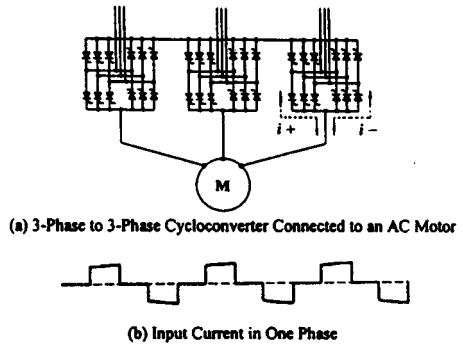

Fig. 15. A 3-phase to 3-phase cycloconverter and its input phase current.

The sideband frequencies vary with the output frequency of the cycloconverter, resulting in a frequency spectrum that changes as the motor speed is adjusted. According to [53], independent of pulse number and circuit configuration, the characteristic harmonics generated by an ideal cycloconverter for single-phase and three-phase outputs are $f_h = f_i \pm 2kf_o$ and $f_h = f_i \pm 6kf_o$, respectively, where $k = 0, 1, 2, \ldots$. f_i and f_o are the input and output frequencies of the cycloconverter, respectively.

For the six-pulse and twelve-pulse cycloconverters with single-phase and balanced three-phase outputs, the dominant harmonic frequencies present in the input current are

$$f_h = |(pm \pm 1) f_i \pm 2kf_o| \tag{22}$$

and

$$f_h = |(pm \pm 1) f_i \pm 6kf_o|, \tag{23}$$

respectively, where $p = 6$ or $p = 12$, and $m = 1, 2, \ldots$. In (22) and (23), the first term specifies the characteristic harmonics from a p-pulse converter and the second term represents sidebands of each of the dominant characteristic harmonics, which may not be integers. In general, the currents associated with the sideband frequencies are relatively small and harmless to the power system unless a sharply tuned resonance occurs at that frequency.

B. Harmonic Models of the Cycloconverter

Since the harmonic frequencies generated by a cycloconverter depend on its changed output frequency, it is very difficult to eliminate them completely. Also, there are little literature on the subject of harmonic analysis and modeling of a cycloconverter under abnormal operations, such as input voltage unbalanced or distorted or nonsinusoidal load currents [54]–[57]. Up to date, the time-domain and current source models are commonly used for modeling harmonic characteristics of cycloconverters. The harmonic currents injected into a power system by cycloconverters still present a challenge to both researchers and industrial engineers.

V. Discussions and Comments

In previous sections, many harmonic models for major power electronic devices have been reviewed, both in the time domain and in the frequency domain. Though there is no consensus on the preference of any specific models for harmonic analysis, bear in mind that an accurate solution for modeling the power

electronic device involves the steady-state interaction between the device and the power system.

Under the assumption of ideal operating conditions, the closed-form solution for modeling the device generally can be obtained or analytically expressed either in time domain or in frequency domain. In reality, the source voltage of a power-electronic device may be unbalanced or distorted. Besides, uneven source impedance (including transformer) and factors that affect the device conduction such as variations in thyristor firing angle control and commutation intervals, all contribute to the generation of noncharacteristic harmonics in addition to characteristic ones. Therefore, comprehensive harmonic models of the device that take into account more realistic conditions are required for correctly prediction of the generated harmonics and the interactions between the device and the source system.

In the frequency domain, the direct method that uses one-step computation of harmonic voltage profiles with the given current source model (injection) provides the easiest way to perform harmonic analysis but may yield unsatisfactory results. Cater to the interactions between aforementioned power electronic devices and the power system are complicated phenomena, the harmonic analysis with iterative techniques becomes necessary. Developing and integrating the accurate device harmonic model into the solution algorithm of the iterative harmonic analysis with good computational efficiency is of great importance. References [58]–[62] provide some detailed insights on convergence criteria for applying such iterative techniques.

In the reviewed time-domain device models, the solution method used is a time simulation of the entire system. The actual periods of operation within each cycle of device operation and the power system are described by differential equations. The solution is obtained by assigning a set of initial conditions for the states of the system and integrating the system equations over time. The solution methods are the most matured. Many commercialized programs have been developed and can be used to obtain a complete time-domain solution. No attempt is made to convert to the frequency domain. Both balanced, unbalanced, and distorted input conditions can be handled, and the device model can be as detailed as necessary. However, the solution time and engineering effort increase significantly. Another disadvantage with the time-domain model is that, conventional load flow constraints may not be able to be considered. In addition, improving computational efficiency and simultaneously modeling of multiple devices in the simulation remains as a challenge.

VI. Conclusion

For an accurate power system harmonic analysis, the adequate models of harmonic sources are required. In this paper, characteristics and modeling of major power electronic harmonic sources are reviewed. Conventionally, the balanced and nondistorted input to the harmonic sources is assumed, and the current source model is sufficient for the representation of the harmonic source. However, under the nonideal input situations, noncharacteristic harmonics are generated and more advanced harmonic models may be necessary for harmonic penetration studies. As described in the paper, many methods for modeling harmonic sources in the frequency and time domains have been proposed, where the nonlinearity of harmonic sources are properly modeled.

Acknowledgment

The Task Force would like to acknowledge the following members for their major contributions: G. Chang (editor), Y. Liu (editor), C. Hatziadoniu, A. Medina, R. Natarajan, T. Ortmeyer, N. Watson, P. Ribeiro, and W. Xu. The support of the IEEE PES Harmonics Working Group chaired by Dr. A. J. F. Keri for this work is also acknowledged.

References

[1] Task Force on Harmonics Modeling and Simulation, "The modeling and simulation of the propagation of harmonics in electric power networks—Part I: Concepts, models and simulation techniques," *IEEE Trans. Power Delivery*, vol. 11, no. 1, pp. 452–465, Jan. 1996.

[2] J. A. Oliver, "Adjustable speed drives: Application guide," EPRI, Palo Alto, CA, Tech. Rep. TR-101 140, Dec. 1992.

[3] N. Mohan, T. M. Undeland, and W. P. Robbins, *Power Electronics—Converters, Applications, and Design*: John Wiley & Sons, 1995.

[4] E. W. Kimbark, *Direct Current Transmission*. New York: Wiley & Sons, 1971, vol. I.

[5] T. H. Ortmeyer, "Harmonic analysis methodology,", IEEE PES Tutorial Course, Course Text 84 EH0221-2-PWR, pp. 74–84,, Feb. 1984.

[6] D. J. Pileggi, N. H. Chandra, and A. E. Emanuel, "Prediction of harmonic voltages in distribution systems," *IEEE Trans. Power Apparatus and Systems*, vol. PAS-100, no. 3, pp. 1307–1315, Mar. 1981.

[7] A. A. Mahmoud and R. D. Shoultz, "A method for analyzing harmonic distribution in AC power systems," *IEEE Trans. Power Apparatus and Systems*, vol. PAS-101, no. 6, pp. 1815–1824, Mar. 1982.

[8] M. F. McGranaghan, R. C. Dugan, and W. L. Sponsler, "Digital simulation of distribution system frequency-response characteristics," *IEEE Trans. Power Apparatus and Systems*, vol. PAS-100, no. 3, pp. 1362–1369, Mar. 1981.

[9] J. Arrillaga, B. C. Smith, N. R. Watson, and A. R. Wood, *Power System Harmonic Analysis*: John Wiley & Sons, 1997.

[10] L. Hu and R. Yacamini, "Harmonic transfer through converters and HVDC links," *IEEE Trans. Power Electronics*, vol. 7, no. 3, pp. 514–524, July 1992.

[11] J. Rittiger and B. Kulicke, "Calculation of HVDC-converter harmonics in frequency domain with regard to asymmetries and comparison with time domain simulations," *IEEE Trans. Power Delivery*, vol. 10, no. 4, pp. 1944–1949, Oct. 1995.

[12] M. Sakui and H. Fujita, "Calculation of harmonic currents in a three-phase converter with unbalanced power supply conditions," *IEE Proc.—Electr. Power Appl.*, vol. 146, no. 1, pp. 478–484, Jan. 1999.

[13] E. Ngandui, G. Olivier, G. April, and A. O. Ba, "Comprehensive switching function approach to calculate harmonics produced by multipulse thyristor converters operating under unbalanced supply," in *Proceedings of the 8th International Conference on Harmonics and Quality of Power*, Oct. 1998, pp. 837–843.

[14] E. V. Larsen, D. H. Baker, and J. C. McIver, "Low-order harmonic interactions on AC/DC systems," *IEEE Trans. Power Delivery*, vol. 4, no. 1, pp. 493–501, Jan. 1989.

[15] A. R. Wood and J. Arrillaga, "The frequency dependent impedance of an HVDC converter," *IEEE Trans. Power Delivery*, vol. 10, no. 3, pp. 1635–1641, July 1995.

[16] S. G. Jalali and R. H. Lasseter, "A study of nonlinear harmonic interaction between a single phase line-commutated converter and a power system," *IEEE Trans. Power Delivery*, vol. 9, no. 3, pp. 1616–1624, July 1994.

[17] N. Rajagopal and J. E. Quaicoe, "Harmonic analysis of three-phase AC/DC converters using the harmonic admittance method," in *Proceedings of IEEE Canadian Conference on Electrical and Computer Engineering*, vol. 1, Sept. 1993, pp. 313–316.

[18] L. Hu and R. E. Morrison, "AC side equivalent circuit-based method for harmonic analysis of a converter system," *IEE Proc.—Electr. Power Appl.*, vol. 146, no. 1, pp. 103–110, Jan. 1999.

[19] A. Semlyen, E. Acha, and J. Arrillaga, "Newton-type algorithms for the harmonic phasor analysis of nonlinear power circuits in periodical steady state with special reference to magnetic nonlinearities," *IEEE Trans. Power Delivery*, vol. 3, no. 3, pp. 1090–1098, July 1988.

[20] W. Xu, J. E. Drakos, Y. Mansour, and A. Chang, "A three-phase converter model for harmonic analysis of HVDC systems," *IEEE Trans. Power Delivery*, vol. 9, no. 3, pp. 1724–1731, July 1994.

[21] W. Xu, H. W. Dommel, M. B. Hughes, G. W. Chang, and L. Tang, "Modeling of adjustable speed drives for power system harmonic analysis," *IEEE Trans. Power Delivery*, vol. 14, no. 2, pp. 595–601, Apr. 1998.

[22] W. Xu, H. W. Dommel, M. B. Hughes, and Y. Liu, "Modeling of DC drives for power system harmonic analysis," *IEE Proc.—Gener. Transm. Distrib.*, vol. 146, no. 3, pp. 217–222, May 1999.

[23] B. C. Smith, N. R. Watson, A. R. Wood, and J. Arrillaga, "Steady state model of the AC/DC converter in the harmonic domain," *IEE Proc.—Gener. Transm. Distrib.*, vol. 142, no. 2, pp. 109–118, Mar. 1995.

[24] ——, "A Newton solution for the harmonic phasor analysis of AC/DC converters," *IEEE Trans. Power Delivery*, vol. 11, no. 2, pp. 965–971, Apr. 1996.

[25] ——, "A sequence components model of the AC/DC converter in the harmonic domain," *IEEE Trans. Power Delivery*, vol. 12, no. 4, pp. 1736–1731, Oct. 1997.

[26] E. V. Larsen, M. Sublich, and S. C. Kapoor, "Impact of stray capacitance on HVDC harmonics," *IEEE Trans. Power Delivery*, vol. 4, no. 1, pp. 637–645, Jan. 1989.

[27] D. L. Dickmander and K. J. Peterson, "Analysis of DC harmonics using the three-pulse model for the intermountain power project HVDC transmission," *IEEE Trans. Power Delivery*, vol. 4, no. 2, pp. 1195–1204, Apr. 1989.

[28] N. L. Shore, G. Andersson, A. P. Canelhas, and G. Asplund, "A three-pulse model of DC side harmonic flow in HVDC systems," *IEEE Trans. Power Delivery*, vol. 4, no. 3, pp. 1945–1954, July 1989.

[29] K. Sadek and M. Pereira, "Harmonic transfer in HVDC systems under unbalanced conditions," *IEEE Trans. Power Systems*, vol. 14, no. 4, pp. 1934–1939, Nov. 1999.

[30] Y. Baghzouz, "An accurate solution to line harmonic distortion produced by ac/dc converters with overlap and dc ripple," *IEEE Trans. Industrial Applications*, vol. 29, no. 3, pp. 536–540, May/June 1993.

[31] D. E. Rice, "A detailed analysis of six-pulse converter harmonic currents," *IEEE Trans. Industrial Applications*, vol. 30, no. 2, pp. 294–304, May 1994.

[32] B. K. Perkins and M. R. Iravani, "Novel calculation of HVDC converter harmonics by linearization in the time-domain," *IEEE Trans. Power Delivery*, vol. 12, no. 2, pp. 867–873, Apr. 1997.

[33] M. Grotzbach and C. Ried, "Investigation of AC/DC converter harmonics by an analytical based time-discrete approach," *IEEE Trans. Power Delivery*, vol. 12, no. 2, pp. 874–880, Apr. 1997.

[34] D. Xia and G. T. Heydt, "Harmonic power flow studies, Part I—Formulation and solution, Part II—Implementation and practical application," *IEEE Trans. Power Apparatus and Systems*, vol. PAS-101, pp. 1257–1270, June 1982.

[35] V. Sharma, R. J. Fleming, and L. Niekamp, "An iterative approach for analysis of harmonic penetration in power transmission networks," *IEEE Trans. Power Delivery*, vol. 6, no. 4, pp. 1698–1706, Oct. 1991.

[36] G. Carpinelli, F. Gagliardi, M. Russo, and D. Villacci, "Generalized converter models for iterative harmonic analysis in power systems," *IEE Proc.—Gener. Transm. Distrib.*, vol. 141, no. 5, pp. 445–451, Sept. 1994.

[37] G. Carpinelli, F. Gagliardi, M. Russo, and A. Sturchio, "Steady-state mathematical models of battery storage plants with line-commutated converters," *IEEE Trans. Power Delivery*, vol. 8, no. 2, pp. 494–503, Apr. 1993.

[38] M. Tou, A. Ba-Razzouk, T. Rafesthain, K. Debebe, and V. Rajagopalan, "Global simulation of multiple power electronic converter system using a novel iterative method," in *Proceedings of the 1992 International Conference on Industrial Electronics, Control, Instrumentation, and Automation*, New York, Nov. 1992, pp. 494–499.

[39] L. Gyugyi and E. R. Taylor, "Characteristics of static, thyristor-controlled shunt compensators for power transmission system applications," *IEEE Trans. Power Apparatus and Systems*, vol. PAS-99, no. 5, pp. 1795–1804, Sept./Oct. 1980.

[40] T. J. Miller, *Reactive Power Control in Electric Systems*. New York: John Wiley & Sons, Inc., 1982.

[41] W. Xu, J. R. Jose, and H. W. Dommel, "A multiphase harmonic load flow solution technique," *IEEE Trans. Power Systems*, vol. PS-6, pp. 174–182, Feb. 1991.

[42] J. Montaño, J. Gutierrez, A. Lopez, and M. Castilla, "Effects of voltage-waveform distortion in TCR-type compensators," *IEEE Trans. Industrial Electronics*, vol. 40, no. 3, pp. 373–383, June 1993.

[43] W. Xu, J. R. Marti, and H. W. Dommel, "Harmonic analysis of systems with static compensators," *IEEE Trans. Power Delivery*, vol. 6, no. 1, pp. 183–190, Feb. 1991.

[44] E. Acha, "Harmonic domain representation of thyristor controlled reactor," in *Proceedings of the 5th International Conference on AC and DC Power Transmission*, London, UK, Sept. 1991.

[45] J. J. Rico, E. Acha, and T. J. E. Miller, "Harmonic domain modeling of three phase thyristor-controlled reactors by means of switching vectors and discrete convolutions," *IEEE Trans. Power Delivery*, vol. 11, no. 3, pp. 1678–1684, July 1996.

[46] E. Acha, J. J. Rico, S. Acha, and M. Madrigal, "Harmonic modeling in Hartley domains," *IEEE Trans. Power Delivery*, vol. 12, no. 4, pp. 1622–1628, Oct. 1997.

[47] L. J. Bohmann and R. H. Lasseter, "Harmonic interactions in thyristor controlled reactor circuits," *IEEE Trans. Power Delivery*, vol. 4, no. 3, pp. 1919–1926, July 1989.

[48] J. J. Rico and E. Acha, "The use of switching function and Walsh series to calculate waveform distortion in thyristor-controlled compensated power circuit," *IEEE Trans. Power Delivery*, vol. 13, no. 4, pp. 1370–1377, Oct. 1998.

[49] C. M. Osauskas and A. R. Wood, "A frequency domain model of a thyristor controlled reactor," in *Proceedings of the 8th International Conference on Harmonics and Quality of Power*, Athens, Greece, Oct. 1998, pp. 923–929.

[50] A. Medina and N. Garcia, "Newton methods for the fast computation of the periodic steady state solution of systems with nonlinear and time-varying components," in *Proceedings of the 1999 PES Summer Meeting*, Edmonton, Canada, July 1999, pp. 664–669.

[51] S. L. Lee, S. Bhattacharya, T. Lejonberg, A. Hammad, and S. Lefebvre, "Detailed modeling of static VAR compensators using the electromagnetic transients program (EMTP)," *IEEE Trans. Power Delivery*, vol. 7, no. 2, pp. 836–847, Apr. 1992.

[52] S. Lefebvre and L. Gérin-Lajoie, "A static compensator model for the EMTP," *IEEE Trans. Power Systems*, vol. 7, no. 2, pp. 477–486, May 1992.

[53] B. R. Pelly, *Thyristor Phase-Controlled Converters and Cycloconverters*: John Wiley & Sons, 1971.

[54] R. F. Chu and J. J. Burns, "Impact of cycloconverter harmonics," *IEEE Trans. Industry Applications*, vol. 25, no. 3, pp. 427–435, May/June 1989.

[55] J. P. Tamby, V. I. John, and P. Chadwick, "A direct optimum symmetry (DOS) spectral calculation method for cycloconverter synchronous motor drive systems," in *Conference Record of 1989 IEEE Industry Applications Society Annual Meeting*, Oct. 1989, pp. 1092–1098.

[56] R. Balasubramanyam and V. I. John, "Spectral calculation software for a circulating current cycloconverter drive system," in *Proceedings of 1993 Canadian Conference on Electrical and Computer Engineering*, Sept. 1993, pp. 437–440.

[57] K. S. Smith and L. Ran, "Input current harmonic analysis of pseudo 12-pulse 3-phase to 6-phase cycloconverters," *IEEE Trans. Power Electronics*, vol. 11, no. 4, pp. 629–640, July 1996.

[58] C. D. Callaghan and J. Arrillaga, "Convergence criteria for iterative harmonic analysis and its applications to static converter," in *Proceedings of the 4th International Conference of Harmonics on Power Systems*, Budapest, Hungary, Oct. 1990, pp. 314–319.

[59] J. Arrillaga and C. D. Callaghan, "Three phase AC–DC load and harmonic flows," *IEEE Trans. Power Delivery*, vol. 6, no. 1, pp. 238–244, Jan. 1991.

[60] R. Carbone, M. Fantauzzi, F. Gagliardi, and A. Testa, "Some considerations on the iterative harmonic analysis convergence," *IEEE Trans. Power Delivery*, vol. 8, no. 2, pp. 487–493, Apr. 1993.

[61] J. G. Mayordomo, R. Asensi, F. Orzáez, M. Izzeddine, and L. Zabala, "Comparative study of algorithms for iterative harmonic analysis and its applications to static converters," in *Proceedings of the 6th International Conference of Harmonics on Power Systems*, Bolgana, Italy, Sept. 1994, pp. 303–310.

[62] B. C. Smith, J. Arrillaga, A. R. Wood, and N. R. Watson, "A review of iterative harmonic analysis for AC–DC power systems," *IEEE Trans. Power Delivery*, vol. 13, no. 1, pp. 180–185, Jan. 1998.